Journal of Education and Science (ISSN 1812-125X)

www.edusj.mosuljournals.com

Magnetite Nanoparticles-Polymer Composites For Effective Adsorption of Ultracidin Pesticide From Water

W. H. Abdulqader [(1)], J. A. Abbas [(2)]

[(1,2)] Department of Chemistry, College of Science, University of Duhok, Duhok, Iraq

Article information

Article history:
Received: January 21, 2024
Accepted: March 14, 2024
Available online: June 01, 2024

Keywords:
Polyacrylic acid
Iron oxide nanoparticles
Ultracidin, Adsorption
Water treatment.

Correspondence:
Walaa H. Abdulqader
walaa.abdulqader@uod.ac

Abstract

In this study, hydrogels of polyacrylic acid (PAA) were synthesised using free radical polymerization of acrylic acid. This process was carried out in an aqueous medium in the existence of ammonium persulfate (APS) acting as an initiator, and N, N'-methylene bisacrylamide (MBA), which is used as a crosslinker. There were four different acrylic acid hydrogel formulations made, and each had a different crosslinker concentration that varied from 0.5 to 2.0 mol% MBA. The next step includes the co-precipitation of PAA7 with iron oxide magnetite nanoparticles (PAA7/Fe_3O_4) for recover the hydrogel from batch mode using a magnetic field once Ultracidin pesticide has been absorbed from aqueous solutions. The adsorbent was characterized by FTIR, VSM, and XRD. The Ultracidin adsorption from an aqueous solution was studied by varying a number of parameters, including pH, contact time, temperature, adsorbent dose, and adsorbate concentration. Best adsorption efficiency was obtained at a temperature of 25°C, 60 minutes of contact time at pH 3, with 50 mg L^{-1}, of initial pesticide concentration, and 4 g L^{-1} adsorbent dose. Several models were used to examine the adsorption kinetics of pesticide onto the adsorbent (PAA7/Fe_3O_4 NPs). The best effect showed that the pseudo second order model correlates with the experimental data. To determine the ideal adsorption capacity of the adsorbent, Langmuir, Freundlich, and Tempkin adsorption isotherms were utilized. Langmuir- model demonstrated a fitter than other models. The outcomes show that Ultracidin can be successfully removed from polluted water using (PAA7/Fe_3O_4 NPs) composite.

DOI: 10.33899/edusj.2024.146255.1420,

1. Introduction

Water contamination is a worldwide environmental affair, and the levels of harmful pollutants present in water sources far override the sill set up by the World Health Organisation (WHO)and the Environmental Protection Agency (EPA) [1]. Water quality is progressively diminishing due to its pollution by various detrimental compounds like agrochemicals, dyes, personal care products (PPCPs), and pharmaceuticals. Within the agricultural and industrial domains, agrochemicals, particularly pesticides and herbicides, are extensively manufactured and applied, leading to the pollution of both surface and groundwater sources [2]. Until now, numerous approaches have been documented for effectively eradicating organophosphorus (Ops) compounds from water solutions. These methods encompass electrochemistry, adsorption, enzymatic biodegradation, and photocatalysis. Among these alternatives, the use of adsorption techniques stands out as a competitive approach due to its straightforward implementation and cost-effectiveness. The pivotal endeavor lies in the creation of novel adsorbents possessing superior adsorption capabilities, a task of paramount importance and complexity in addressing the ongoing issue of persistent Ops pollution within the environment [3]. Pesticides have the potential to enter the body through different pathways, including inhaling aerosols, dust, and vapors that have been contaminated with pesticides; by consuming

food or water that has been contaminated, as well as through direct contact with the skin [4]. Methidathion is indeed an active ingredient used in some pesticides, including Ultracidin. It's classified as an organophosphate insecticide and deviates from other organophosphates in its toxicity characteristics. Due to its relatively elevated fat solubility, methidathion exhibits a notably extensive distribution throughout the body. This characteristic indicates that hemoperfusion is ineffective in eliminating this particular organophosphate from the body [5].

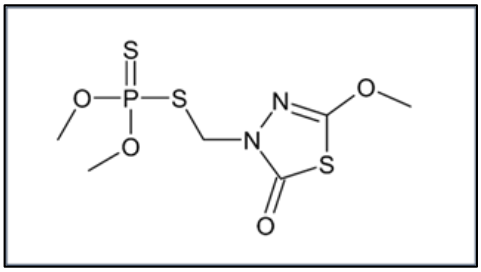

Figure 1. Methidathion (3-dimethoxyphosphinothioylthiomethyl-5-methoxy-1,3,4-thiadiazol-2(3H)-one) [6].

Methidathion poses a significant risk of both acute and chronic poisoning. Methidathion is currently categorized in Schedule 7 of the Standard for the Uniform Scheduling of Drugs and Poisons (SUSDP), with no lower schedule entries available for diluted preparations. This classification aligns with its categorization internationally. It has received a classification of being highly hazardous from the World Health Organization (WHO), the European Union (EU), and the US Environmental Protection Agency (US EPA), which both classify it as extremely dangerous [7,8].

One of the techniques that could be used as adsorbents is polymer. Polyacrylic acid (PAA) is an economically feasible polymer commonly utilized in commercial applications. Typically, it is formed through the polymerization process of acrylic acid monomers. This polymer is characterized by its non-toxic, biocompatible, and biodegradable properties. Enhanced mechanical properties through the cross-linking of PAA and to form a stable structure [9]. The typical method of creating PAA is through free radical polymerization using a suitable initiator, as shown in Figure 2 [10].

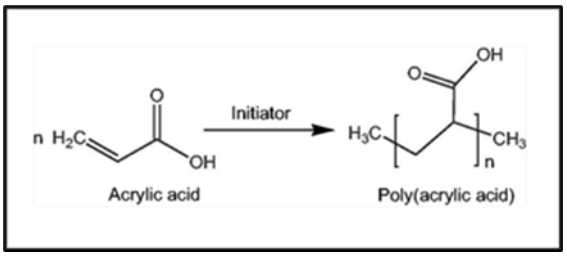

Figure 2. Polymerization reaction of acrylic acid.

The use of magnetic materials in water purification provides a solution to the challenges associated with filtering and renewing adsorbents. As a result, numerous researchers have extensively developed and employed magnetic materials for effectively treating pollutants [11,12].

Magnetic iron oxide nanoparticles (NPS) have a high degree of recyclability and reusability and are non-toxic. Furthermore, their magnetic behavior offers the advantage of facile separation when an external magnetic field is applied. According to recent research, precipitation and co-precipitation techniques have been widely used for NP synthesis. The production of iron oxide may be accomplished quickly, easily, and affordably with the co-precipitation approach. [13].

The purpose of the current study is to examine the PAA7/Fe_3O_4 nanocomposite's adsorption behavior for removing pesticides from solutions of water, such as Ultracidin-40%EC. Indeed, the persistent use of banned pesticides like Methidathion in Iraq underscores a critical environmental challenge, leading to significant water pollution concerns. The goal of the study is to identify the ideal circumstances for achieving the maximum Ultracidin-40% EC elimination. These parameters include the pH, contact duration, adsorbent dose, and initial pesticide concentration. The maximum adsorption capacity (Q_m) and other adsorption process constants were found using a variety of isotherm models. Because kinetic models are important for figuring out the reaction process, they were taken into consideration. These conditions include initial pesticide concentration, adsorbent dosage, contact time, and pH. The highest capacity for adsorption (Q_m) and other adsorption process constants were found using a variety of isotherm models. Because kinetic models are important for figuring out the reaction process, they were taken into consideration.

2. Substances and synthesis

2.1 Substances

Acrylic acid (AAc) (99%), and N, N'- methylene bisacrylamide (MBA) (99%) were supplied from Himedia. 98% of (APS) ammonium persulphate and NaOH 96% supplied by Merck. $FeCl_3.6H_2O$ and $FeSO_4.7H_2O$ were supplied from UNI-CHEM chemical reagents. NH_4OH (30%) was supplied from Panreac, HCl (37%) was supplied from Scharlau. Ultracidin-40% was supplied from Vapco Company, Jordan. 1000 mg L^{-1} of Ultracidin stock solution prepared via dissolving Ultracidin-40% in distilled water.

This solution was employed for the subsequent preparation of experimental solutions. NaOH or HCl was used to modify the pH values. A pH meter calibrated with buffer solutions of pH 4, 7, and 10 was employed. The concentration of Ultracidin in the adsorption solutions was measured using a spectrophotometer.

2.2 Synthesis of Polyacrylic acid hydrogels (PAA)

Aground, 16 hydrogel formulations from PAA and NaPAA were prepared, employing the various synthesis methods outlined subsequently. The Table (1) contains a summary of hydrogel forms. By using the solution polymerization process, four formulae of PAA hydrogels with different crosslinker percentages (0.5 to 2.0 mol% MBA) were prepared. As outlined in Table (1), AAc, APS, and different concentrations of MBA have been dissolved in distilled water. Subsequently, they were vigorously mixed at room temperature up till uniform. After 10 minutes of nitrogen gas purging to eliminate air bubbles, each solution was put into silicone-coated glass tubes. The glass tubes were then sealed and put in a 60°C water bath. After 25 minutes, gelation appeared. To ensure a complete reaction, the polymerization process was allowed to continue for 150 minutes. The hydrogels underwent a 48-hour rinsing process with distilled water following their synthesis, with water replaced every 12 hours, to eliminate unreacted ingredients. The hydrogels were then filtered through filter paper and dry a whole day for a full day at 80 °C in a vacuum drying oven. Using a crusher and pestle, the dried hydrogels were crushed into smaller pieces.

2.3 Sodium-poly acrylic acid hydrogel (NaPAA)

With various crosslinker ratios (0.5–2.0 mol%) of MBA and (30–100 mol%) of AAc neutralized, twelve different NaPAA hydrogel formulations were prepared (Table 1). As will be described below by equation (1), the percentage of neutralization was calculated using the ratio of moles of NaOH to moles of AAc. The preparation of NaPAA hydrogels involved mixing 200 g.L^{-1} of AAc with a preset quantity of NaOH in D.W. The solution was stirred until the heat caused by neutralization had diminished. Subsequently, at room temperature, 2 g.L^{-1} of APS and preset quantities of MBA were completely mixed as well as dissolved till the mixture achieved homogeneity.

Identical procedures employed in the synthesis, drying, and purification of PAA hydrogels, as mentioned in the preceding section, were then conducted [14].

$$\text{The percentage of AAc neutralization} = \frac{\text{mol NaOH}}{\text{mol AAc}} \text{x} 100 \qquad (1)$$

$$\text{The percentage of Crosslinker to AAc} = \frac{\text{mol MBA}}{\text{mol AAc}} \text{x} 100 \qquad (2)$$

2.4 Synthesis of PAA/Fe_3O_4 NPs

PAA-coated MNPs were prepared by the coprecipitation technique, as described in the references [15, 16]. In summary, 160 mL of D.W. was used to dissolve 4.9 g of $FeSO_4$. $7H_2O$ and 9.5 g of $FeCl_3$. $6H_2O$ at 55°C in a nitrogen (N_2) environment. 1.26 g of PAA was added, and vigorous stirring was done for 30 minutes. Afterward, 1.26 g of PAA was added, followed by 30 minutes of vigorous stirring. Following that, 10 mL of NH_4OH was rapidly added, causing the colour to turn from orange to black. The PAA7/Fe_3O_4 nanocomposites were separated using a magnet and then washed with distilled water till the pH was neutral. They were then dried in a vacuum drying oven for 12 hours at 75°C. Finally, the PAA/Fe_3O_4 NPs were subsequently grinded and stored for later use in glass containers that were tightly sealed.

Table1. A summary of the various PAA and NaPAA hydrogel formulations

Name of Sample	Sample Number	Mole Percentage of AAc neutralization	Mole percentage of MBA /AAc	NaOH (g/25ml)	MBA (g/25ml)
PAA	1	0	0.5	0	0.0534
	2	0	1	0	0.1068
	3	0	1.5	0	0.1604
	4	0	2	0	0.2136
NaPAA30	5	30	0.5	0.832	0.0534
	6	30	1	0.832	0.1068
	7	30	1.5	0.832	0.1604
	8	30	2	0.832	0.2136
NaPAA60	9	60	0.5	1.664	0.0534
	10	60	1	1.664	0.1068
	11	60	1.5	1.664	0.1604
	12	60	2	1.664	0.2136
NaPAA100	13	100	0.5	2.773	0.0534
	14	100	1	2.773	0.1068
	15	100	1.5	2.773	0.1604
	16	100	2	2.773	0.2136

2.5 Characterization

A variety of techniques were used for evaluating the characteristics of PAA7, Fe_3O_4, and PAA7/Fe_3O_4 NPs as well as investigating their adsorption mechanisms. An Analytical diffractometer, X'Pert, high-score X-ray (PW1730, Philips, Netherlands) employing Cu-Kα1 radiation (λ = 1.540598 Å) was used to determine the crystalline size of the adsorbents. The parameters included k, which is Scherer's constant (0.94), β representing (FWHM), the full width at half maximum of the peak, and θ, indicating the diffraction angle at 30 mA and 40 kV, a range of 2θ was acquired between 10 - 80. The Debye-Scherer mode was used to compute the crystallite size, D = (kλ / β cos θ) [17]. The Vibrating Sample Magnetometer (VSM1100, WEISTRON - Taiwan) was utilized to examine the magnetic characteristics of the nanoparticles. FT-IR spectra for PAA7, Fe_3O_4, PAA7/Fe_3O_4, and the Ultracidin-loaded PAA7/Fe_3O_4 were obtained using an FT-IR spectrometer (1800-SHIMADZU, Japan) between 400 and 4000 cm^{-1} in the wavenumber range.

3. Studies on the Batch absorption

3.1 pH's effect on adsorption

Adsorption experiments in solutions with Acidity levels 1, 3, 5, 7, and 9 were conducted. Acidity and alkalinity of the medium were regulated by adding the necessary quantities of hydrochloric acid and sodium hydroxide solutions. The influence of the initial pH, on the adsorption of Ultracidin, onto the adsorbent was assessed and the results are presented in Table (3). All batch tests took samples from duplicate flasks filtered with the qualitative filter paper 102 mild. The filtrate's residual Ultracidin concentration was then measured. The amount of Ultracidin taken per gram of adsorbent, q_e mg/g, was computed using the following equation:

$$q_e = \frac{(C_i - C_e) \times V}{m} \qquad (3)$$

In this case, C_i stands for Ultracidin's initial concentration, C_e is equilibrium liquid-phase concentrations (mg/L), V is the solution's volume (L), and m is the weight (g) of the adsorbent that was utilized.

The following formula was used to get the amount of Ultracidin removal (R %):

$$R\% = \frac{(C_i - C_e)}{C_i} \times 100 \qquad (4)$$

3.2 Effect of the initiating concentration of Ultracidin

Experiments using various starting Ultracidin concentrations ranging between 25 to 100 $mg.L^{-1}$ were carried out to ascertain the effect of Ultracidin amount on the removal percentage and adsorption capacity. All other factors were kept constant. The results are presented in Table (5).

3.3 Effect of contact time

Kinetic studies were carried out in a pH 3 solution by agitating 4 $g.L^{-1}$ of PAA7/Fe_3O_4 NPs in a 50 ($mg.L^{-1}$) solution of the Ultracidin at 25°C. The batch tests were carried out across a range of times. Table (6) contains the Ultracidin adsorption data.

3.4 Adsorbent dose's effect

The effects of dose on the removal of 50 ($mg.L^{-1}$) Ultracidin was studied using different concentration of (PAA7/Fe_3O_4 NPs), at 25°C, pH 3, for 1 h, and agitation rate 150 RPM Table (4).

3.5 Adsorption isotherm

Experiments on adsorption isotherms were conducted at various temperatures with various initial concentrations of Ultracidin. The adsorbent dose and pH were kept constant. All isotherm experiments were done with a linear thermostat shaker, and the results are reported in Table (8).

4. Results and Discussion

4.1 Characterization

A powder X-ray diffractometer was employed to gather diffraction data for the Fe_3O_4 and PAA7/Fe_3O_4 samples during the examination. The data was collected using a position-sensitive, X'Celerator detection system, with a step size of 0.05° and a range of 10.24 to 70.99°, using continuous scanning mode. For calculating the average grain size of magnetic nanoparticles, the Scherrer equation was employed, as shown below:

$$D_p = (K \lambda) / (\beta \cos \theta) \quad (5)$$

Where: D_p represents the mean grain size, λ is the X-ray wavelength (1.5406 Å), β is the full width at half maximum intensity (FWHM expressed in radians), and θ is the diffraction angle at 40 kV and 30 mA. k is the shape-dependent Scherrer's constant (0.94). The Scherrer equation was used to analyze crystal size, and the results showed that Fe_3O_4 had a crystal size of (5.37 to 11.11 nm) and PAA7/Fe_3O_4 had a size (2.5 to 11.05 nm) that was almost identical to Fe_3O_4 Fig. (3). Iron oxide nanoparticles' magnetic hysteresis loop Fig. (4) was plotted versus magnetic field and mass magnetization ratio (M). The value of M_s, which quantifies the maximum magnetic strength, was determined to be 52.53 emu/g for Fe_3O_4 and 45.3 emu/g for PAA7/Fe_3O_4, respectively. M_s values for both nanoparticles are lower than for pure magnetite (Fe_3O_4), which has a value of 92 emu/g [18]. This decrease in magnetization didn't affect external magnet attraction since PAA7/Fe_3O_4 remained firmly attracted to the external magnet. The coercivities (H_c) for Fe_3O_4 and PAA7/Fe_3O_4 are -8.646 and 0.96 O_e, respectively. The ferromagnetic nature of the nanoparticles is shown by these values. The residual magnetization (M_r) of Fe_3O_4 and PAA7/Fe_3O_4 is 0.888 and -0.077 emu/g, respectively Table (7). Consequently, PAA7/Fe_3O_4 will respond to an external magnetic field with these magnetization values leading to the separation of the polymer composite (PAA7/Fe_3O_4) loaded with Ultracidin-40%EC from an aqueous solution.

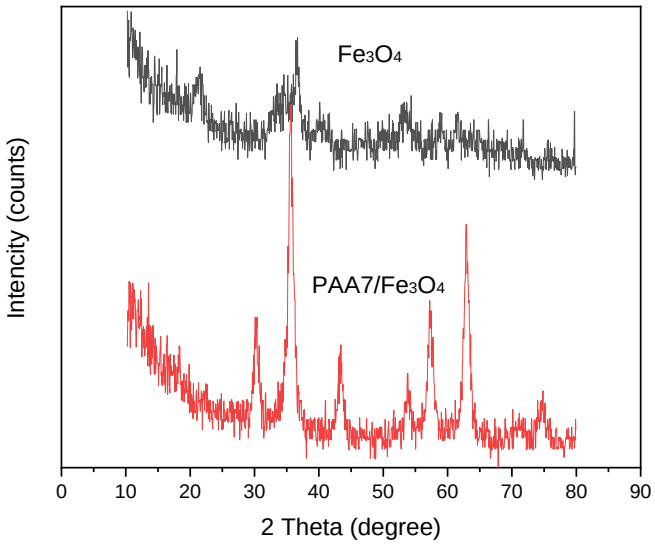

Figure 3. XRD distribution of Fe_3O_4 and AC/Fe_3O_4.

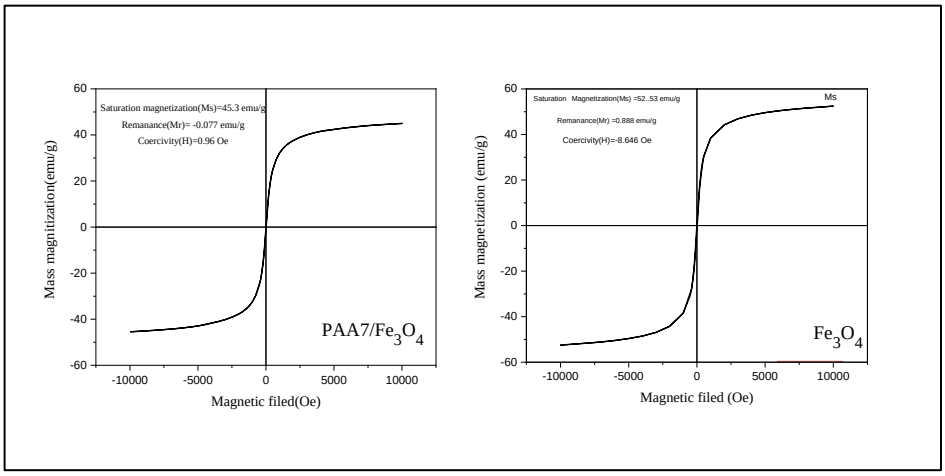

Figure 4 . Magnetic moment loop of Fe_3O_4 and AC/Fe_3O_4

Table 2. Shows the magnetic properties of Fe_3O_4 and PAA7/Fe_3O_4.

Nanoparticles	Saturation magnetization (emu/g)	Remnant magnetization (emu/g)	Coercivity (O_e)
Fe_3O_4	52.53	0.888	-8.646
PAA7/Fe_3O_4	45.3	-0.077	0.96

The functional groups and associated frequencies are displayed in the FT-IR spectra of Fe_3O_4, PAA7, PAA7/Fe_3O_4, Ultracidin-40%EC, and Ultracidin-40%EC-loaded PAA7/Fe_3O_4, Fig. (5). The bands observed within the range of 613.36 to 478.35 cm^{-1} indicate the formation of magnetic nanoparticles, especially connected to the distinctive Fe–O stretching band on their surface. The spectra further displayed stretching vibrations of water molecules (free O–H) of Fe_3O_4 at 3159.40 cm^{-1}. This vibration observed in the spectrum could be attributed to residual moisture present in KBr and the particles. The carbonyl group inside (-COOH)group, is responsible for the vibration of the peak shown at 1732 cm^{-1}, whereas C–O groups are peaking at 1450 cm^{-1}[14,19,20]. In the Ultracidin-40%EC spectrum, the peaks of 1176 cm^{-1} , and 1585 cm^{-1} correspond to the C−N and the C=N bonds respectively [21,22]. The weak absorption peak at 690 cm^{-1} was caused by the (C–S) bond stretching vibration, whereas a significant absorption band at 1014 cm^{-1} was formed by the vibration of the P–O–C bond. The stretching vibration for C-H bond was identified as the cause of the absorption peaks that were detected in the 3012–2843 cm^{-1} range [23, 24]. Upon Ultracidin's adsorption over the surface of PAA7/Fe_3O_4, changes in transmission and a displacement of the peak were also noted.

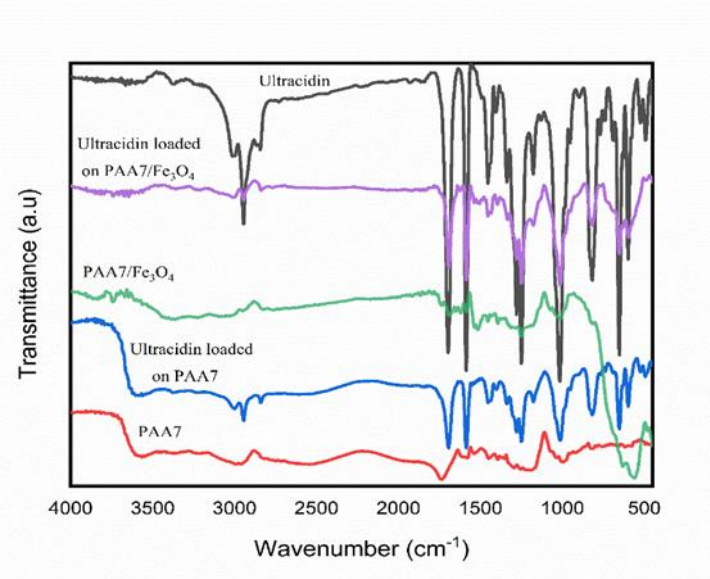

Figure 5. FTIR spectra of Ultracidin, polyacrylic acid/Fe_3O_4 after Ultracidin adsorption, Polyacrylic acid/Fe_3O_4, Poly acrylic acid after Ultracidin adsorption, and Poly acrylic acid sample 7.

4.2 pH-dependent studies

The effect of the pH on the Ultracidin adsorption, using PAA7/Fe_3O_4, was examined to identify the optimal adsorption pH of the pesticide mentioned above, in the pH range of 1-9. All other process factors were taken into consideration while assessing the pH values, including the initial pesticide concentration (50 mg/L), PAA7/Fe_3O_4 dose (4g.L^{-1}), the temperature (25°C), shaking rate(150 RPM) and (1h) contact time were kept constant. Fig. (6) displays that maximum removal of the pesticide 81.29% was achieved at pH 3.0 and It was noted that, the removal of pesticide decreased from 65 to 62% as pH was increased from 5 to 9.

Table 3. Efficacy of pH on Ultracidin adsorption (50 mg.L^{-1}) solution, upon 4g.L^{-1} of (PAA7/Fe_3O_4) NPs, for 60 min. at 25°C and 150 RPM of agitation rate.

pH	C_e (mgL^{-1})	q_e (mgL^{-1})	R%
1	9.5962	10.10095	80.8076
3	9.3531	10.1617	81.2939
5	17.4926	8.12685	65.0148
7	18.3171	7.92072	63.3658
9	18.9937	7.75158	62.0127

4.3 The effect of adsorbent dosage

The composite quantity of (PAA7/Fe_3O_4 NPs) varied between 2 and 8 $g.L^{-1}$. The initial Ultracidin concentration of 50 mg/L, one-hour contact period, the pH of 3, and 25 degrees Celsius were all maintained as constants. Table (4) and Fig. (7) show the concluded data. It demonstrates that higher adsorbent doses result in higher removal efficiencies. This is an expected result. With higher adsorbent dosage, there are more active sites available, allowing a greater number of Ultracidin molecules to adsorb onto these active sites, which results in a discernible improvement in removal effectiveness. which leads to a noticeable increase in removal efficiency [25]. At 8 gL^{-1}, the highest removal of Ultracidin (R %) via PAA7/Fe_3O_4 NPs was 93.19%. In contrast, at a dosage of 2 g/L, it was 71.6%.

Table 4. The effects of dosage on the elimination of 50 $mg.L^{-1}$ Ultracidin was studied using different dosages of (PAA7/Fe_3O_4 NPs), at 25°C, pH 3, for 1 h, and agitation speed 150 RPM.

PAA7/Fe_3O_4 NPs, conc. ($g.L^{-1}$)	C_e ($mg.L^{-1}$)	q_e ($mg.g^{-1}$)	R%
2	14.1839	8.95402	71.6321
4	9.37421	10.1565	81.2516
6	5.92812	11.0179	88.1438
8	3.40169	11.6496	93.1966

4.4 Effect of initial concentration

The initial Ultracidin concentration was adjusted from 25 to 100 $mg.L^{-1}$ while maintaining the other parameters, which included a pH of 3, an hour of contact, and 4 $g.L^{-1}$ of adsorbent concentration at 25°C. The results corresponding to these conditions are depicted in Fig. (8) and Table (5). Pesticide molecule removal efficiency from the medium remained consistently above 80% up to 75 $mg.L^{-1}$ a concentration. This suggests the presence of an ample number of active sites available for effective adsorption within this range. Nevertheless, the adsorption process is adversely affected by concentration increases up to 100 mg/L, which lowers removal efficiency. This decline occurs when the available sites become insufficient and equilibrium has already been attained [26].

Table 5. The effect of initiating concentration on Ultracidin's adsorption onto (PAA7/Fe_3O_4 NPs) 4$g.L^{-1}$ was investigated at pH 3 for 60 min. at 25°C and 150 RPM of agitation.

C_i mg L^{-1}	C_e (mg L^{-1})	q_e (mg g^{-1})	R %
25	4.68076	5.07981	81.2769
50	9.37421	10.1564	81.2516
75	14.4165	15.1459	80.7780
100	26.6977	18.3256	73.3023

4.5 The effect of the contact time

The pesticide adsorption from (50 $mg.L^{-1}$) an aqueous solution onto 4 $g.L^{-1}$ of the investigated adsorbent (PAA7/Fe_3O_4 NPs) was examined at various contact times, ranging from 15 to 180 minutes.

The results of this investigation are reported in Table, (6) and Fig. (9). Ultracidin's adsorption capabilities increase in the first sixty minutes and achieve equilibrium adsorption in around eighty minutes. The outcome was explained by the fact that there were initially empty sites in the composite when the adsorption process started. After these sites filled up progressively, the adsorption rate decreased over time until it reached its maximal adsorption capacity [3,27].

Table 6. The effect of contact time on the adsorption of Ultracidin, 50 mg.L^{-1} solution, onto (PAA7/Fe_3O_4 NPs), 4g L^{-1}, at 25°C, pH 3, and agitation rate 150 RPM.

Time (min)	C_e (mg L^{-1})	q_t (mg g^{-1})	q_e-q_t (mg g^{-1})	log(qe-qt) (mg g^{-1})	t/q_t (min g mg-^{1})	ln t (min)	$t^{1/2}$ (min$^{1/2}$)	R%
15	21.48	7.127	4.172	0.620	2.104	2.708	3.872	57.02
30	20.07	7.482	3.818	0.581	4.009	3.401	5.477	59.85
60	9.331	10.16	1.133	0.054	5.901	4.094	7.745	81.33
90	7.556	10.61	0.689	-0.161	8.481	4.499	9.486	84.88
120	5.293	11.17	0.124	-0.905	10.73	4.787	10.95	89.41
150	5.103	11.22	0.076	-1.115	13.36	5.010	12.24	89.79
180	4.797	11.30			15.92	5.192	13.41	90.40

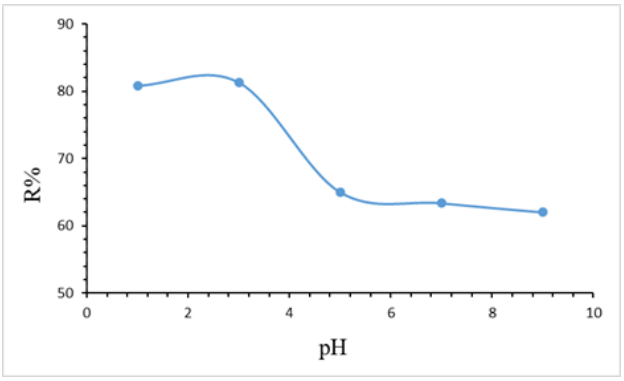

Figure 6. The effect of the pH on the adsorption of 50 mg.L^{-1} , Ultracidin solution, onto 4g.L^{-1} adsorbent (PPA7/Fe_3O_4 NPs).

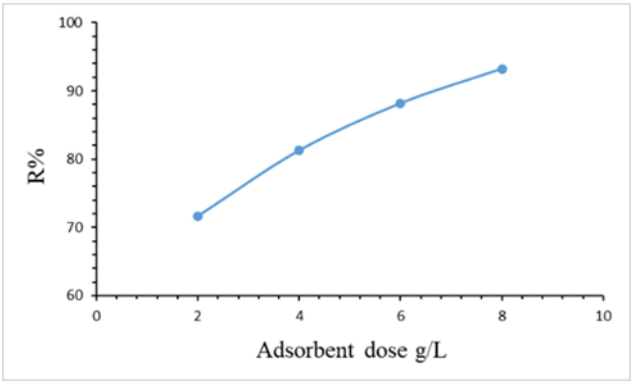

Figure 7. The effect of the adsorbent dose (PPA7/Fe_3O_4 NPs) on the Ultracidin removal, R%.

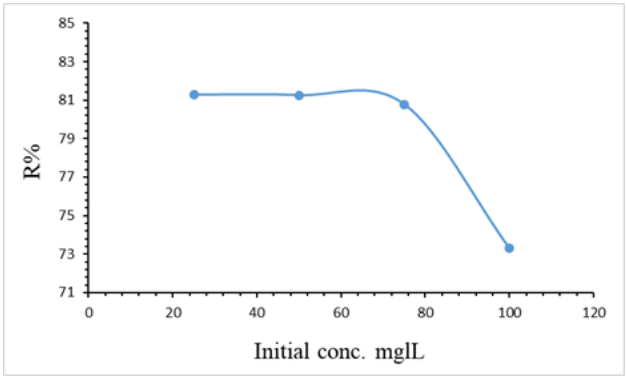

Figure 8. The effect of the amount of Ultracidin adsorbed at equilibrium, using (PPA7/Fe_3O_4 NPs) 4g.L^{-1}, at pH 3, time 60 min., temp. 25°C, R% vs. initial conc

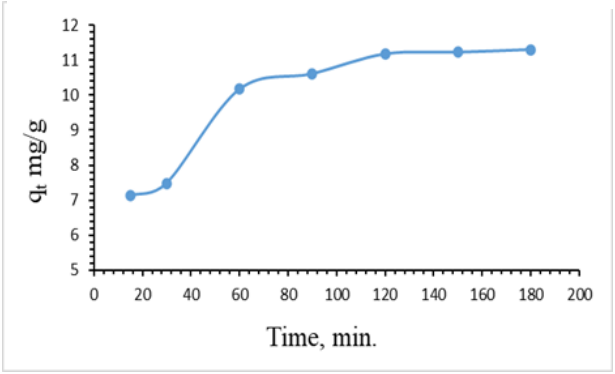

Figure 9. The effect of the contact time on Ultracidin removing using (PPA7/Fe_3O_4 NPs) 4g.L^{-1}, at pH 3, temp. 25°C, q_t vs. Time.

4.6 Adsorption kinetic

To gain a more profound understanding of the adsorption of Ultracidin pesticides onto PAA7/Fe_3O_4 NPs (considered the most effective adsorbent in this study), data on pesticide adsorption was collected over time. This data was subsequently fitted to several models of kinetic,(pseudo-first-order, pseudo-second-order, intraparticle diffusion kinetic, and Elovich),

represented by equations (6, 7, 8, and 9). This comprehensive analysis allows for a more detailed assessment of the adsorption process.

$$log(q_e - q_t) = log\, q_e - \frac{k_1 t}{2.303} \quad (6)$$

$$t/q_t = \frac{1}{k_2 {q_e}^2} + \frac{1}{q_e}(t) \quad (7)$$

$$q_t = (\frac{1}{\beta}) ln(\alpha\beta) + \frac{1}{\beta} ln(t) \quad (8)$$

$$q_t = k_{dif}\, t^{1/2} + B_L \quad (9)$$

where; (q_e) is the adsorption capacity at equilibrium ($mg.g^{-1}$), and (q_t) is at the duration time; K_1 in the pseudo-first-order model, refers to the rate constant of adsorption (min^{-1}) , k_2, in the pseudo-second-order refers to, initial adsorption rate ($mg.g^{-1}.min^{-1}$) ; α and β represent the adsorption rate constants in the Elovich model; k_{dif} is the constant of intraparticle diffusion rate ($mg.g^{-1}.min^{-0.5}$), In the intraparticle diffusion model, B_L is the intercept that indicates to ,the adsorbent material's boundary layer thickness, [28]. Table (7) lists the correlation coefficients and kinetic parameters, while Figures (10,11,12, and 13) show the corresponding fitting plots. The pseudo 2^{nd}-order kinetic , displayed a greater coefficient of linear regression ($R^2 = 0.998$) in comparison to the pseudo-1^{st}-order kinetic ($R^2 = 0.973$). As the outcome, pseudo -2^{nd}- order model is considered to be the most appropriate of describing the process of the adsorption. The predicted values obtained from the previous model and the experimental results also show a significant degree of agreement, indicating that this model is better appropriate for explaining the kinetics of Ultracidin pesticide adsorption on the ($PAA7/Fe_3O_4$ NPs) composite. These findings suggest that the concentrations of the pesticide and the adsorbent are related to the rate-determining step of the pesticide's adsorption on the ($PAA7/Fe_3O_4$ NPs) composite [29]. A further model of linear kinetics, known as the Elovich model, was also investigated. This is valuable for characterizing non-uniform solid surface order. The values of α and β were obtained by plotting q_t versus ln(t), displayed in Fig. (12) and Table (7). This model's parameters are commonly used to describe the adsorption behavior of pollutants on heterogeneous adsorbents and in processes that require high activation energy. The activation energy is predicted to alter by the surface coverage if the sites are distributed heterogeneously. [30,31]. With an R^2 value of 0.934, the Elovich model demonstrates a reasonably good fit and validity for describing the adsorption process. To comprehensively understand the adsorption kinetics, the rate of the controlling phase was also determined using the intraparticle diffusion kinetic model. This primarily depends on the external or the pore diffusion mechanisms. The connection between q_t and t½ should be linear and pass through the origin. The diffusion has a major effect on adsorption as the rate-determining step. Plots of q_t versus t½ reveal two separate linear segments, as Fig. (13) illustrates, indicating that the diffusion process proceeds in two phases. The plot's intercept represents the influence of the boundary layer, where a greater intercept suggests a more substantial contribution of the boundary layer effect to the rate-controlling step [26,3].

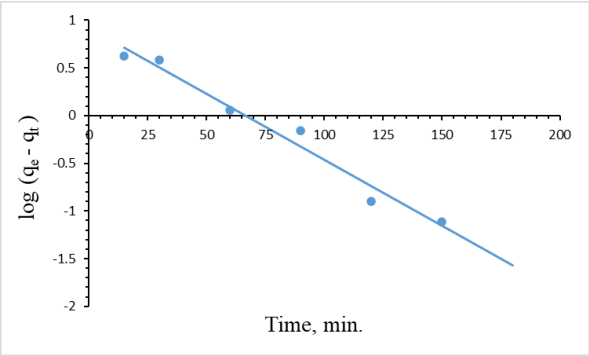

Figure 10. Pseudo 1st order kinetics of Ultracidin adsorption upon (PPA7/Fe_3O_4 NPs).

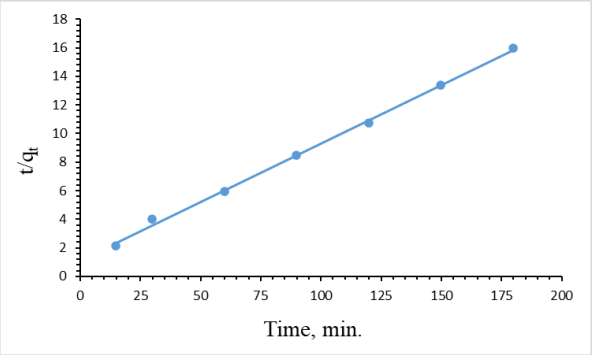

Figure 11. Pseudo 2nd order kinetics of Ultracidin adsorption upon (PPA7/Fe_3O_4 NPs).

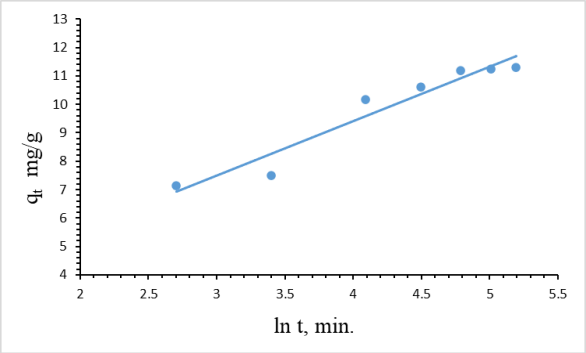

Figure 12. Elovich, kinetic of Ultracidin adsorption upon (PPA7/Fe_3O_4 NPs).

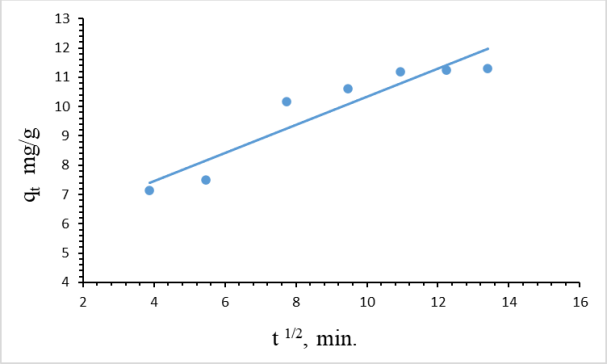

Figure 13. Intraparticle diffusion, kinetic of Ultracidin adsorption upon (PPA7/Fe_3O_4 NPs).

Table 7. Adsorption of Ultracidin, 50 mg/L, onto (PPA7/Fe_3O_4 NPs), 4g/L, at constant temperature (25°C) and varied times, compared with calculated experimental q_e values, using different models.

Kinetic models	Parameter	
Pseudo First - order kinetic	q_e , exp. (mg g^{-1})	11.30074
	k_1($min.^{-1}$)	0.03178
	q_e , calc. (mg g^{-1})	8.2129
	R^2	0.9733
Pseudo Second - order kinetic	k_2 ,(g.$mg^{-1}min^{-1}$)	0.005917
	h, (mg. g^{-1} min^{-1})	0.8886
	q_e ,calc.(mg g^{-1})	12.2549
	R^2	0.998
Elovich	β ,(g mg^{-1})	0.5214
	α ,(mg. g^{-1} min^{-1})	4.7386
	R^2	0.9344
Intraparticle diffusion	$K_{diff.}$,(mg. g^{-1} $min^{-0.5}$)	0.4804
	B_L ,(mg g^{-1})	5.5323
	R^2	0.8827

4.7 Adsorption isotherm

The equilibrium behavior of adsorbents at constant temperature is explained by the adsorption isotherm. It depends on some physical characteristics of the solution, including pH, temperature, and ionic strength, as well as the characteristics of the adsorbed species, the adsorbent, and the adsorbate. Adsorption isotherms often arise when there is enough contact between the adsorbent and the adsorbate over some time such that the concentration of the adsorbate in the bulk solution and the interface concentration achieve a dynamic equilibrium. Adsorption isotherms are often used in the characterisation of porous materials and the design of commercial adsorption systems. [32]. To achieve which of the three isotherms might best explain the experimental findings, an evaluation was conducted on the Langmuir, Freundlich, and Temkin isotherms. Equations (10, 11, 12, and 13) are used to express these isotherms.

$$\frac{1}{q_e} = (\frac{1}{K_L Q_m})\frac{1}{C_e} + \frac{1}{Q_m} \quad (10)$$

$$log\, q_e = log\, K_F + \frac{1}{n} log\, C_e \quad (11)$$

$$q_e = B_T\, ln\, A_T + B_T\, ln\, C_e \quad (12)$$

$$B_T = \frac{RT}{b_T} \quad (13)$$

The equilibrium concentration, C_e, is expressed in ($mg.L^{-1}$) in the Langmuir isotherm equation. The quantity adsorbed at equilibrium, q_e, is expressed in ($mg.g^{-1}$). The maximum Langmuir adsorption capacity is represented by Q_m. The constant K_F in the Freundlich equation ($mg.g^{-1}$) indicates the adsorption capacity. Meanwhile, n (measured in $L.mg^{-1}$) stands for the adsorption intensity, measuring the change in affinity of the adsorbate with alterations in adsorption density. The Temkin constants in the Temkin equation are B_T and A_T ($L.mg^{-1}$). In addition, the constant b_T is connected to the heat of adsorption, T stands for the temperature in Kelvin, and R is 8.314 $J.mol^{-1}.K^{-1}$ [33]. Langmuir's isotherm explains the monolayer adsorption of Ultracidin contaminants onto the (PAA7/Fe_3O_4 NPs) composite surface, considering the surface contains a limited number of active sites that are capable of the adsorption, On the other hand, the Freundlich model suggests that adsorption occurs on the adsorbent's heterogeneous surface. According to Temkin's isotherm, the uniform distribution of binding energies up to a maximum binding energy characterizes adsorption, and the heat of adsorption progressively decreases as molecules of the adsorbate cover the surface of the adsorbent. [26]. Figures (14, 15, and 16) Display the experiment findings along with their corresponding fitting lines for a range of pesticide starting concentrations that were evaluated at different temperatures. The appropriateness of the isotherm equation is randomly determined using the linear regression coefficient, or R^2 [29]. The information in Table (9) demonstrates that Langmuir's isotherm provides a more suitable fit than the Freundlich and Temkin models.

Table- 8. The following are the equilibrium conditions for the adsorption of Ultracidin onto (PAA7/Fe_3O_4 NPs): 4 mg/L, pH 3, 60 minutes, and 150 RPM of agitation.

At 25°C

C_i ($mg.L^{-1}$)	C_e ($mg.L^{-1}$)	q_e ($mg.g^{-1}$)	log C_e ($mg.L^{-1}$)	Log q_e ($mg.g^{-1}$)	Ln C_e ($mg.L^{-1}$)	1/ C_e ($L.mg^{-1}$)	$1/q_e$ ($g.mg^{-1}$)
25	4.680	5.079	0.670	0.705	1.543	0.213	0.196
50	9.374	10.15	0.971	1.006	2.237	0.106	0.098
75	14.41	15.14	1.158	1.180	2.668	0.069	0.066
100	26.69	18.32	1.426	1.263	3.284	0.037	0.054

At 35°C

C_i ($mg.L^{-1}$)	C_e ($mg.L^{-1}$)	q_e ($mg.g^{-1}$)	Log C_e ($mg.L^{-1}$)	Log q_e ($mg.g^{-1}$)	Ln C_e ($mg.L^{-1}$)	$1/C_e$ ($L.mg^{-1}$)	$1/q_e$ ($g.mg^{-1}$)
25	5.093	4.976	0.706	0.696	1.627	0.196	0.200
50	12.18	9.453	1.085	0.975	2.500	0.082	0.105
75	20.70	13.57	1.316	1.132	3.030	0.048	0.073
100	31.30	17.17	1.495	1.234	3.443	0.031	0.058

At 45°C

C_i (mg/L)	C_e ($mg.L^{-1}$)	q_e ($mg.g^{-1}$)	Log C_e ($mg.L^{-1}$)	Log q_e ($mg.g^{-1}$)	Ln C_e ($mg.L^{-1}$)	$1/C_e$ ($L.mg^{-1}$)	$1/q_e$ ($g.mg^{-1}$)
25	5.283	4.929	0.722	0.692	1.664	0.189	0.202
50	18.86	7.783	1.275	0.891	2.937	0.053	0.128
75	21.64	13.33	1.335	1.125	3.074	0.046	0.074
100	39.69	15.07	1.598	1.178	3.681	0.025	0.066

At 55°C

C_i ($mg.L^{-1}$)	C_e ($mg.L^{-1}$)	q_e ($mg.g^{-1}$)	Log C_e ($mg.L^{-1}$)	Log q_e ($mg.g^{-1}$)	Ln C_e ($mg.L^{-1}$)	$1/C_e$ ($L.mg^{-1}$)	$1/q_e$ ($g.mg^{-1}$)
25	6.033	4.741	0.780	0.675	1.797	0.165	0.210
50	21.30	7.172	1.328	0.855	3.059	0.046	0.139
75	34.39	10.15	1.536	1.006	3.537	0.029	0.098
100	43.39	14.15	1.637	1.150	3.770	0.023	0.070

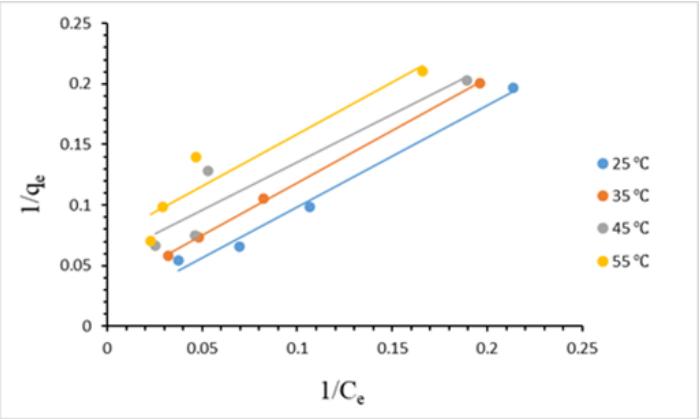

Figure 14. The Langmuir isotherm shows the temperature dependence of ultracidin's adsorption upon (PPA7/Fe_3O_4 NPs).

Table 9. Comparison of the coefficient isotherm parameters from Ultracidin adsorption onto (PPA7/Fe_3O_4 NPs).

Isotherm model	Isotherm parameter	Temperature °C			
		25	35	45	55
Langmuir	Q_m (mg/ g)	68.96	30.95	17.793	13.679
	K_L (L.mg $^{-1}$)	0.017	0.037	0.0711	0.085
	R^2	0.987	0.999	0.8866	0.893
Freundlich	K_F	1.749	1.652	1.8767	1.7803
	n	1.327	1.453	1.7658	1.9662
	R^2	0.945	0.997	0.866	0.9118
Tempkin	A_T	0.413	0.384	0.4545	0.4293
	B_T	7.852	6.659	5.013	4.1239
	b_T	315.5	384.5	527.39	661.27
	R^2	0.982	0.983	0.8055	0.8022

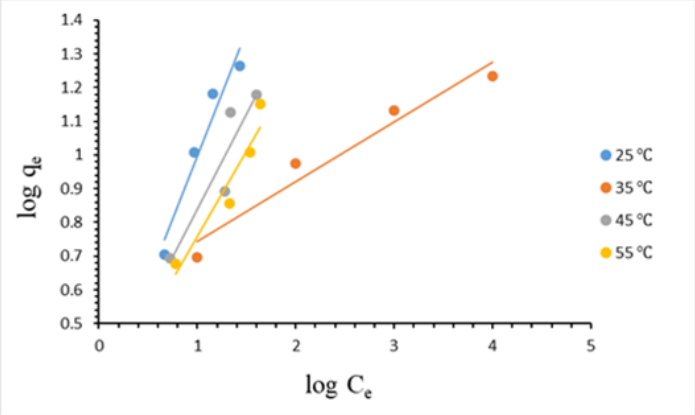

Figure 15. Freundlich isotherm showing the different temperatures at which Ultracidin adsorbs upon (PPA7/Fe_3O_4 NPs).

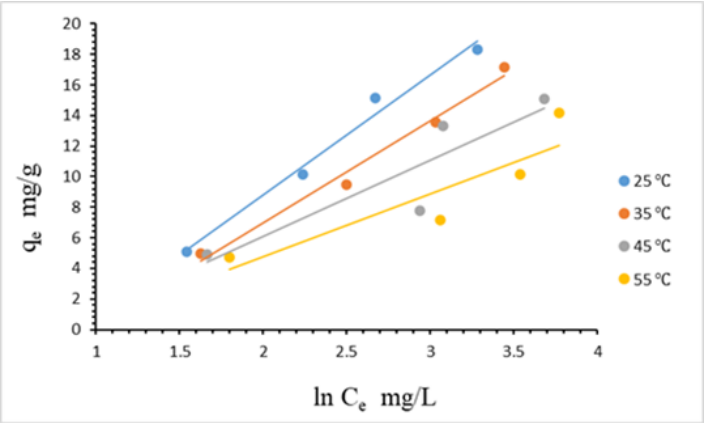

Figure 16. The Tempkin isotherm illustrates how Ultracidin adsorbs onto (PPA7/Fe_3O_4 NPs) at different temperatures.

5. Conclusion

The composite (PAA7/Fe_3O_4 NPs) was successfully synthesized in this study. This combination was used as an adsorbent to effectively separate Ultracidin from water-based solutions using the coprecipitation technique. A reaction temperature of 25°C and a period time of 180 minutes were found to be the ideal parameters for attaining maximal Ultracidin absorption. The absorbent exhibited high sensitivity to pH, demonstrating multiple adsorptions of Ultracidin across a pH range from 1 to 9. The maximum removal of Ultracidin, achieved with 4 g/L of absorbent reached 81.29% at pH 3. The kinetics of adsorption followed the pseudo 2nd order model. In comparison to the Freundlich and Tempkin models, the Langmuir model offers a superior match to the equilibrium data. Given these results, it can be concluded that (PAA7/Fe_3O_4 NPs) can be efficiently, economically, and environmentally friendly utilized for the purification of water from Ultracidin. This research advances environmental theory by showcasing effective methods for removing Methidathion from water and indicates the potential for developing commercially viable purification technologies. Furthermore, it facilitates the translation of findings into policies and practices to address pesticide pollution and promote sustainable water management. Additionally, this study underscores the substantial environmental repercussions of this pesticide. This research offers valuable insights into purifying Ultracidin-contaminated water, yet it has limitations. The laboratory-scale approach may not fully represent real-world conditions, affecting the efficacy of purification techniques in larger field settings. Additionally, assuming homogeneous conditions for pollutant distribution and water quality parameters may not accurately reflect the heterogeneity of natural water bodies.

6. Acknowledgment

The authors would like to thank the Duhok University Department of Chemistry for providing all the materials needed to complete this study. The authors are not connected to any organization that has an interest in the paper's subject matter financially, either directly or indirectly.

7. References

[1] Lingamdinne LP, Koduru JR, Karri RR, "A comprehensive review of applications of magnetic graphene oxide based," *Journal of Environmental Management*, vol. 231, pp. 622–634, 2019, https://doi.org/10.1016/j.jenvman.2018.10.063

[2] Mondol MM, Jhung SH, "Adsorptive removal of pesticides from water with metal–organic framework-based materials," *Chemical Engineering Journal*, vol. 421, no. Part 1, pp. 129688, 2021. https://doi.org/10.1016/j.cej.2021.129688

[3] Zhu X, Li B, Yang J, Li Y, Zhao W, Shi J, Gu J, "Effective adsorption and enhanced removal of organophosphorus

pesticides from aqueous solution by Zr-based MOFs of UiO-67.," *ACS applied materials & interfaces,* vol. 7, no.1, pp. 223-231., 2015, https://doi.org/10.1021/am5059074

[4] Bhandari S, Paneru S, Pandit S, Rijal S, Manandhar HK, Ghimire BP, "Assessment of pesticide use in major vegetables from farmers'perception and knowledge in Dhading district, Nepal.," *Journal of Agriculture and Natural Resources* , vol. 3, no.1, pp. 265-281 , 2020, DOI: https://doi.org/10.3126/janr.v3i1.27180

[5] Kim KH, Kim SH, Her C, "Methidathion poisoning," *Korean Journal of Critical Care Medicine* , vol. 32, no. 4, pp.363-369, 2017, https://doi.org/10.4266/kjccm.2016.00073

[6] Hladik ML, Orlando JL. Level 1 Water-quality Inventory of Baseline Levels of Pesticides in Urban Creeks: Golden Gate National Recreation Area and the Presidio of San Francisco, California., U.S. Geological Survey, 2008, URL: https://pubs.usgs.gov/ds/338

[7] Singh S, Sharma N, " Neurological syndromes following organophosphate poisoning.," *Neurology India* , vol. 48, no. 4, pp. 308, 2000.

[8] Yamashita M, Tanaka J, Ando Y, "Human mortality in organophosphate poisonings," *Veterinary and human toxicology* , vol. 39, no. 2, pp. 84-85, 1997, https://europepmc.org/article/med/9080632

[9] Kausar A, "Poly (acrylic acid) nanocomposites: Design of advanced materials," *Journal of Plastic Film & Sheeting* , vol. 37, no. 4, pp. 409-428, 2021, https://doi.org/10.1177/8756087920981615

[10] Gavasane AJ, Pawar HA, "Synthetic biodegradable polymers used in controlled drug delivery system: an overview," *Clin Pharmacol Biopharm* , vol. 3, no. 2, pp. 1-7, 2014. http://dx.doi.org/10.4172/2167-065X.1000121

[11] Reddy DH, Lee SM, "Three-dimensional porous spinel ferrite as an adsorbent for Pb (II) removal from aqueous solutions," *Industrial & Engineering Chemistry Research* , vol. 52, no. 45, pp. 15789-15800, 2013, https://doi.org/10.1021/ie303359e

[12] Reddy DH, Lee SM, "Application of magnetic chitosan composites for the removal of toxic metal and dyes from aqueous solutions," *Advances in colloid and interface science* , vol. 201, pp. 68-93, 2013, https://doi.org/10.1016/j.cis.2013.10.002

[13] Abdullah NH, Shameli K, Abdullah EC, Abdullah LC, "Solid matrices for fabrication of magnetic iron oxide nanocomposites: synthesis, properties, and application for the adsorption of heavy metal ions and dyes," *Composites Part B: Engineering,* , vol. 162, pp. 538-568, 2019. https://doi.org/10.1016/j.compositesb.2018.12.075

[14] Cruz H, Laycock B, Strounina E, Seviour T, Oehmen A, Pikaar I, "Modified poly (acrylic acid)-based hydrogels for enhanced mainstream removal of ammonium from domestic wastewater," *Environmental Science & Technology* , vol. 54, no. 15, pp. 9573-9583, 2020. https://doi.org/10.1021/acs.est.9b07032

[15] Lin CL, Lee CF, Chiu WY, "Preparation and properties of poly (acrylic acid) oligomer stabilized superparamagnetic ferrofluid," *Journal of Colloid and Interface Science,* vol. 291, no. 2, pp. 411-420, 2005, https://doi.org/10.1016/j.jcis.2005.05.023

[16] Sanchez LM, Martin DA, Alvarez VA, Gonzalez JS, "Polyacrylic acid-coated iron oxide magnetic nanoparticles: The polymer molecular weight influence," *Colloids and Surfaces A: Physicochemical and Engineering Aspects* , vol. 543, pp. 28-37, 2018, https://doi.org/10.1016/j.colsurfa.2018.01.050

[17] Iqbal J, Shah NS, Sayed M, Imran M, Muhammad N, Howari FM, Alkhoori SA, Khan JA, Khan ZU, Bhatnagar A, Polychronopoulou K, "Synergistic effects of activated carbon and nano-zerovalent copper on the performance of hydroxyapatite-alginate beads for the removal of As3+ from aqueous," *Journal of Cleaner Production,* vol. 235, pp.

875886, 2019, https://doi.org/10.1016/j.jclepro.2019.06.316

[18] Dunlop DJ, Özdemir Ö. Rock magnetism: fundamentals and frontiers, Cambridge university press, 1997.

[19] Businova P, Chomoucka J, Prasek J, Hrdy R, Drbohlavova J, Sedlacek P, Hubalek J, "Polymer coated iron oxide magnetic nanoparticles: preparation and characterization," *Nanocon* , vol. 9 , pp. 21-23, 2011.

[20] Lin CL, Lee CF, Chiu WY, "Preparation and properties of poly (acrylic acid) oligomer stabilized superparamagnetic ferrofluid," *Journal of Colloid and Interface Science* , vol. 291, no. 2, pp. 411-420, 2005, https://doi.org/10.1016/j.jcis.2005.05.023

[21] Li ZY, Horn F, Li Y, Mou LH, Schöllkopf W, Chen H, He SG, Asmis KR, "Dinitrogen Activation in the Gas Phase: Spectroscopic Characterization of C− N Coupling in the V3C++ N2 Reaction," *Chemistry–A European Journal* , vol. 29, no. 14, pp. e202203384, 2023. https://doi.org/10.1002/chem.202203384

[22] Traxler M, Gisbertz S, Pachfule P, Schmidt J, Roeser J, Reischauer S, Rabeah J, Pieber B, Thomas A, "Acridine-Functionalized Covalent Organic Frameworks (COFs) as Photocatalysts for Metallaphotocatalytic C− N Cross-Coupling," *Angewandte Chemie International Edition,* vol. 61, no. 21, pp. e202117738, 2022, https://doi.org/10.1002/anie.202117738

[23] Coates J, "Interpretation of infrared spectra, a practical approach," 2000.

[24] Cheng Y, Guo X, Xue Y, Pang H, "Controllable synthesis of a flower-like superstructure of nickel metal-organic phosphate and its derivatives for supercapacitors," *Applied Materials Today* , vol. 23 , pp. 101048, 2021, https://doi.org/10.1016/j.apmt.2021.101048

[25] Baharum NA, Nasir HM, Ishak MY, Isa NM, Hassan MA, Aris AZ, "Highly efficient removal of diazinon pesticide from aqueous solutions by using coconut shell-modified biochar, " Highly efficient removal of diazinon pesticide from aqueous solutions by using coconut shell-modified biochar," *Arabian Journal of Chemistry,* vol. 13, no. 7, pp. 6106-6121, 2020. https://doi.org/10.1016/j.arabjc.2020.05.011

[26] Sanad MM, Gaber SE, El-Aswar EI, Farahat MM, "Graphene-magnetite functionalized diatomite for efficient removal of organochlorine pesticides from aquatic environment," *Journal of Environmental Management* , vol. 330, pp. 117145, 2023, https://doi.org/10.1016/j.jenvman.2022.117145

[27] Farghali RA, Sobhi M, Gaber SE, Ibrahim H, Elshehy EA, "Adsorption of organochlorine pesticides on modified porous Al30/bentonite: Kinetic and thermodynamic studies," *Arabian Journal of Chemistry* , vol. 13, no. 8, pp. 6730-6740, 2020, https://doi.org/10.1016/j.arabjc.2020.06.027

[28] Fu Q, Jia X, Zhang S, Zhang J, Sun-Waterhouse D, Wang C, Waterhouse GI, Wu P, " Highly defective copper-based metal-organic frameworks for the efficient adsorption and detection of organophosphorus pesticides: An experimental and computational investigation," *Food Chemistry,* vol. 423, pp. 136319, 2023, https://doi.org/10.1016/j.foodchem.2023.136319

[29] Ayub A, Raza ZA, Majeed MI, Tariq MR, Irfan A, "Development of sustainable magnetic chitosan biosorbent beads for kinetic remediation of arsenic contaminated water," *International journal of biological macromolecules,* vol. 163, pp. 603-617 , 2020. https://doi.org/10.1016/j.ijbiomac.2020.06.287

[30] Hidayat AR, Sulistiono DO, Murwani IK, Endrawati BF, Fansuri H, Zulfa LL, Ediati R, "Linear and nonlinear isotherm, kinetic and thermodynamic behavior of methyl orange adsorption using modulated Al2O3@ UiO-66 via acetic acid," *Journal of Environmental Chemical Engineering,* vol. 9, no. 6, pp. 106675, 2021,

https://doi.org/10.1016/j.jece.2021.106675

[31] Pintor AM, Vieira BR, Santos SC, Boaventura RA, Botelho CM, "Arsenate and arsenite adsorption onto iron-coated cork granulates," *Science of the total environment* , vol. 642, pp. 1075-1089, 2018. https://doi.org/10.1016/j.scitotenv.2018.06.170

[32] Al-Ghouti MA, Da'ana DA, "Guidelines for the use and interpretation of adsorption isotherm models: A review," *Journal of hazardous materials* , vol. 393, pp. 122383, 2020, https://doi.org/10.1016/j.jhazmat.2020.122383

[33] Ayawei N, Ebelegi AN, Wankasi D, "Modelling and interpretation of adsorption isotherms," *Journal of chemistry* , vol. 2017, 2017, https://doi.org/10.1155/2017/3039817

إمتزاز مبيد الألتراسيدين بكفاءة من الماء بإستخدام مركب البوليمر مع الجسيمات النانوية المغناطيسية

ولاء حماد عبدالقادر*[1] ، جمال الياس عباس[2]

[1*،2] قسم الكيمياء، كلية العلوم، جامعة دهوك، دهوك، العراق

الخلاصة:

في هذه الدراسة تم تصنيع هيدروجيلات حمض البولي أكريليك (PAA) عن طريق بلمرة الجذور الحرة لحمض الأكريليك. تم تنفيذ هذه العملية في وسط مائي بوجود فوق كبريتات الأمونيوم (APS) والذي يعمل كبادئ و'N،N- ميثيلين بيساكريلاميد (MBA) كرابط تشابك. حضرت أربع تركيبات هيدروجيل PAA، تحتوي كل منها على محتوى تشابكي مختلف تتراوح من 0.5 إلى 2.0 مول% MBA. تضمنت الخطوة التالية الترسيب المشترك لـ PAA7 مع جسيمات أكسيد الحديد النانوية المغناطيسية ($PAA7/Fe_3O_4$) ولأجل إزالة الهيدروجيل من المحاليل المائية بعد إنتهاء عملية الإمتزاز يستخدم مجال مغناطيسي لهذا الغرض. تم تشخيص المادة المازة بإستخدام تقنية FTIR، VSM، وXRD. تمت دراسة امتزاز Ultracidin من المحلول المائي عن طريق تغيير عدد من العوامل، منها الرقم الهيدروجيني، زمن التلامس، درجة الحرارة، جرعة المادة المازة، وتركيز المادة الممتزة. تم الحصول على أفضل كفاءة امتزاز عند درجة حرارة 25 درجة مئوية، بعد 60 دقيقة من وقت التلامس عند PH 3، مع تركيز أولي للمبيد قدره 50 ملجم / لتر وجرعة ممتزة قدرها 4 جم / لتر. تم استخدام عدة نماذج لفحص حركية امتزاز المبيد على المادة المازة ($PAA7/Fe_3O_4$ NPs). أظهرت النتائج أن نموذج الدرجة الثانية الزائفة كان له أفضل ارتباط مع البيانات التجريبية. لتحديد قدرة الامتزاز المثالية للمادة المازة، تم استخدام متساوي حرارة الامتزاز لانجمير وفريندليتش وتمبكين. أظهر نموذج لانجمير توافقًا أفضل بين النماذج الأخرى. أظهرت النتائج إمكانية إزالة الألتراسيدين بنجاح من المياه الملوثة باستخدام مركب ($PAA7/Fe_3O_4$ NPs).